Effect of Cooperative Hydrogen Bonding in Azo−Hydrazone Tautomerism of Azo Dyes

Alimet Sema Özen,* Pemra Doruker, and Viktorya Aviyente

Faculty of Engineering and Natural Sciences, Sabanci University, Orhanli, 34956 Tuzla, Istanbul, Turkey, Department of Chemical Engineering and Polymer Research Center, Bogazici University, 34342 Bebek, Istanbul, Turkey, and Department of Chemistry, Bogazici University, 34342 Bebek, Istanbul, Turkey

Received: July 16, 2007; In Final Form: October 16, 2007

Azo−hydrazone tautomerism in azo dyes has been modeled by using density functional theory (DFT) at the B3LYP/6-31+G(d,p) level of theory. The most stable tautomer was determined both for model compounds and for azo dyes Acid Orange 7 and Solvent Yellow 14. The effects of the sulfonate group substitution and the replacement of the phenyl group with naphthyl on the tautomer stability and on the behavior in solvent have been discussed. Intramolecular hydrogen bond energies have been estimated for the azo and hydrazone tautomers to derive a relationship between the tautomer stability and the hydrogen bond strength. The transition structures for proton transfer displayed resonance assisted strong hydrogen bonding properties within the framework of the *electrostatic-covalent hydrogen bond model* (ECHBM). Evolution of the intramolecular hydrogen bond with changing structural and environmental factors during the tautomeric conversion process has been studied extensively by means of the atoms-in-molecules (AIM) analysis of the electron density. The bulk solvent effect was examined using the self-consistent reaction field model. Special solute−solvent interactions were further investigated by means of quantum mechanical calculations after defining the first-solvation shell by molecular dynamics simulations. The effect of cooperative hydrogen bonding with solvent molecules on the tautomer stability has been discussed.

Introduction

Textile industry wastewater contains unfixed azo dye residuals. Their removal or conversion into potentially harmless substances has been an environmental problem not only because these dyes are relatively resistant to conventional treatment methods but also because some of them produce carcinogenic amines as byproducts of hydrolysis. The most effective solution to this problem is to introduce advanced oxidation processes (AOP),[1−5] where highly reactive hydroxyl radicals generated chemically, photochemically, radiolytically or sonolytically are used as oxidizing agents for the bleaching and mineralization of troublesome waste.

The chromophore structure of azo dyes contains two aryl rings connected through an azo bridge, Ar−N═N−Ar.[6] The chemical and physical characteristics of the dye, like solubility or color, show variance due to the presence of different groups as substituents on the rings. During an advanced oxidation process, the main reactions of hydroxyl radicals with azo compounds are therefore addition to the chromophore, hydrogen abstraction or one-electron oxidation.[3] Experimentally proposed degradation mechanisms focus on the cleavage of either the N−N bond resulting in nitrosoaryl intermediates or the C−N bond with generation of benzene as one of the intermediate products (1).[7,8]

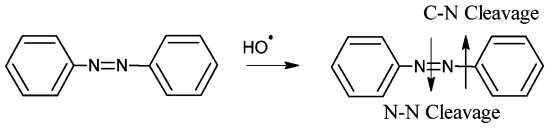

(1)

Azo dyes are known to exist in different tautomeric forms. The presence of at least one protic donor group in conjugation to the azo bridge leads to a prototropic equilibrium that is generally referred to as the azo−hydrazone tautomerism.[6,9−11] This kind of an equilibrium in azo compounds was first postulated by Liebermann[12] in 1883 by assertion of a labile hydroxyl proton in 1-phenylazo-2-naphtol (C.I. Solvent Yellow 14) that is capable of bonding with a nitrogen atom of the azo group (2).

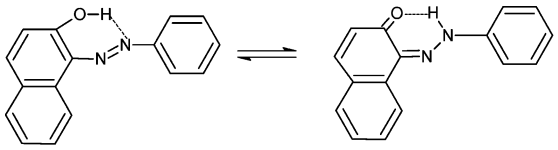

(2)

C.I. Solvent Yellow 14

In our previous studies,[13] hydroxyl radical addition to a variety of the azo dyes was modeled using DFT and it was reported that bleaching of the dye occurs through the attack on N atom followed by the cleavage of the N−N bond rather than the cleavage of the C−N bond in the case of azo tautomers. On the other hand, oxidative degradation of azo dyes that are known to exist preferably in their hydrazone forms was shown to follow a different mechanism, where the adduct formation occurred through the attack of hydroxyl radical to the carbon atom bearing the azo linkage. It was concluded that the presence of the hydrazone tautomer under experimental conditions would point out the degradation via the C−N bond cleavage.[13a] Furthermore, hydrogen abstraction and addition to the ring reactions were found to compete with bond cleavage through addition reactions.[13b,c]

The present study aims to elucidate the mechanism of the azo−hydrazone tautomerism and to investigate the structural (substituent effect) and environmental (solvent effect) factors controlling the preference of one tautomer over the other using

10.1021/jp0755645 CCC: $37.00
Published on Web 12/05/2007

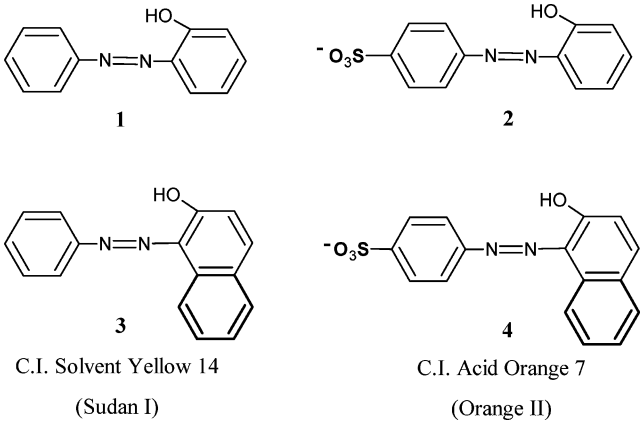

Figure 1. Hydroxy azo dyestuff structures investigated in this study, shown in azo form for convenience.

density functional theory calculations. This information can be used in designing efficient advanced oxidation processes minimizing the production of harmful side products.

Intramolecular proton transfer during azo−hydrazone tautomerism has the features of *resonance assisted hydrogen bonding* (RAHB) within the realm of the electrostatic-covalent hydrogen bond model (ECHBM) proposed by Gilli et al.[14] Consequently, evolution of the intramolecular hydrogen bond with changing structural and environmental factors during the tautomeric conversion process is a predominant central motif in the framework of the present discussion, and a useful tool for understanding tautomerism, studied extensively using the atoms-in-molecules (AIM) theory.[15] Special focus is assigned to the cooperative hydrogen bonding, where the effects of the intermolecular hydrogen bonds with the solvent molecules overlap with the intramolecular hydrogen bonding of the dye molecule.

Compounds **1**−**4** have been chosen as model compounds in this study because they represent the most common structures among azo dyes (Figure 1). Many azo dyes have either benzene or naphthalene frameworks connected through an azo linkage. It is very likely to have di- or trisulfonate substituted azo compounds and the presence of a sulfonate group introduces water solubility. Sulfonate substituted Acid Orange 7 (**4**) is slightly soluble in cold water whereas Solvent Yellow 14 (**3**) is not soluble neither in cold nor in hot water.[16]

Methodology and Theoretical Background

The Gaussian03[17] program has been employed for the evaluation of geometries and energies. Optimizations were performed at the B3LYP/6-31+G(d,p) level of theory. Ground state and transition state structures have been confirmed by frequency analyses at the same level. Transition structures have been characterized by having one imaginary frequency that belonged to the reaction coordinate, corresponding to a first-order saddle point. Zero point vibrational energies (ZPEs) were calculated but not scaled because they would only be used for comparative purposes. Continuum solvent effects were modeled using the integral equation formalism (IEF) polarized continuum model (PCM) of Tomasi et al.[18] within self-consistent reaction field (SCRF) theory, by means of both optimizations and single-point calculations based on the gas-phase geometries.

Molecular dynamics (MD) calculations were performed using ESFF (extensible systematic force field[19]) implemented in Insight II and Discover3.[20] ESFF is a rule-based force field designed for modeling organic, inorganic, and organometallic systems. The usage of ab initio calculated fundamental atomic parameters and application of physical models significantly reduced the fitting parameters and enhanced the accuracy of the ESFF force field. The atomic parameters depend not only on the atom type but also on the specific type that reflects the unusual bonding environments. For example, hydrogen atoms bonded to highly electronegative elements such as O, N, and F will have a different atom type than the nonpolar hydrogen atom bonded to a less electronegative element. In this way, various intramolecular hydrogen bonds of the peptides predicted by the ESFF force field have been found to be in good agreement with experiment.[19] This force field is also a good candidate for simulating conjugated, aromatic, and heterocyclic systems. The initial structures of the molecules were constructed by the BUILDER module and then subjected to a brief energy minimization. Periodic boundary conditions were applied for solvent simulations using the AMORPHOUS_CELL module with dimensions of $20 \times 20 \times 20$ Å^3 and by employing the standard Insight waterbox water model, followed by energy minimization. MD simulations were carried out in the NVT ensemble for 1 ns using a time-step of 1 fs. The temperature of the system was kept at 298 K using direct velocity scaling, and the initial velocities were assigned from Boltzmann distribution. During the simulations, the cutoff distance for nonbonded interactions was taken as 9.50 Å with spline and buffer widths of 1 and 0.5 Å, respectively.

Data obtained from MD calculations were used to locate the explicit water molecules around the azo dye molecule. Supermolecules generated by this method were further optimized at the B3LYP/6-31+G(d,p) level of theory and placed in continuum. Frequency analyses were also performed at the same level of theory.

Atoms-in-molecules (AIM) theory[15] has been employed to reveal the nature of the intramolecular and intermolecular interactions in the course of azo−hydrazone tautomerism. AIM theory is an extension of quantum mechanics to subdomains properly defining an atom as an open system. These subdomains are regions of space bounded by a surface of zero flux in the gradient vector field of the charge density $\nabla\rho(\vec{r})$, and their properties are predicted by quantum mechanics. Every trajectory of $\nabla\rho(\vec{r})$ originates and terminates at a critical point in this field, a point where $\nabla\rho(\vec{r}) = 0$. A critical point with coordinate r_c is characterized by the number of nonzero eigenvalues of the associated Hessian matrix, the matrix of second derivatives of $\nabla\rho(r_c)$, which determines its rank r, and the algebraic sum of their signs, which determines its signature s. For example, a bond critical point (bcp) is a saddle point with 3 nonzero eigenvalues (rank = 3), which correspond to maxima in two directions and a minimum in one direction (signature = −1) and it is represented as (3, −1).

Interatomic interactions can be classified as shared or closed-shell interactions using AIM theory parameters. Accordingly, a shared (covalent) interaction is one where the Laplacian of electron density, $\nabla^2\rho(r)$, at the (3, −1) bond critical point is negative (electron concentration) with a $\rho(r)$ value on the order 10^{-1} au (0.675 e Å^{-3}).[16] A closed-shell (noncovalent) interaction is one where $\nabla^2\rho(r)$ is positive (electron depletion) with a $\rho(r)$ value on the order 10^{-2} au (0.068 e Å^{-3}), which is lower than the former case. There are also intermediate interactions where there is a positive $\nabla^2\rho(r)$ value with a reasonably high $\rho(r)$. According to these definitions, ionic bonds, hydrogen bonds, bonds in van der Waals molecules, and noble gas clusters are closed-shell interactions, whereas covalent or polar bonds are shared interactions.

TABLE 1: Thermodynamic Properties in the Gas Phase and Energetics in Solution for Azo (a) and Hydrazone (h) Tautomers and Proton-Transfer Transition States (TS) for Compounds 1−4 (Relative Energies in kcal/mol[a])

	ΔE	ΔE_{ZPC}	ΔH^{298}	ΔG^{298}	% (298.15 K)	$\Delta E_{solvent}$
1a	−4.98	−2.41	−2.17	−2.82	99.8	−3.82
1TS	0	0	0	0		0
1h	−1.71	0.75	0.98	0.53	0.2	−2.26
2a	−4.27	−1.72	−1.50	−1.98	97.1	−3.88
2TS	0	0	0	0		0
2h	−1.56	0.88	1.11	0.10	2.9	−2.38
3a	−2.57	−0.10	0.17	−0.46	18.2	−1.86
3TS	0	0	0	0		0
3h	−3.70	−0.97	−0.71	−1.35	81.8	−4.45
4a	−2.45	0.00	0.20	−0.06	22.9	−1.49
4TS	0	0	0	0		0
4h	−3.43	−0.66	−0.44	−0.78	77.1	−4.52

[a] 0.00 kcal/mol in the relative energy data corresponds to the following transition states [in Hartrees and in the format of (B3LYP/6-31+G(d,p), IEFPCM//B3LYP)]: 1TS = (−648.029495, −648.021182), 2TS = (−1271.331064, −1271.406587), 3TS = (−801.684872, −801.673116), 4TS = (−1424.985236, −1425.058707).

Wavefunction files were generated within Gaussian 03 using the (output=wfn) option, before being analyzed for the electron density and topological critical points using the AIM2000 implementation of Bader's AIMPAC suite of programs (Biegler-König et al.[21]).

Molecular graphs have been drawn using the program MOLEKEL Version 4.3.win32[22]

Results and Discussion

Structural Factors Controlling the Azo−Hydrazone Tautomerism. Table 1 summarizes the relative energies and thermodynamic properties for the stationary points located on the potential energy profiles of compounds **1**−**4**. Inclusion of zero-point vibrational energy causes the hydrogen to resonate above the intrinsic barrier for proton transfer in some cases. This is a case observed in no-barrier hydrogen bonds.[23] Percent populations of the tautomers, calculated using the Boltzmann distribution, are also shown in this table.

As is clear from Table 1, the azo tautomers **1a** and **2a** are preferred over the hydrazone forms **1h** and **2h** by 3.3 and 2.7 kcal/mol, respectively. On the other hand, replacement of the phenyl groups in **1** and **2** by naphthyl groups in compounds **3** and **4** has shifted the equilibrium toward the hydrazone form. In these latter cases, the two tautomeric forms are isoenergetic and the potential energy surfaces are more symmetric. These findings can be explained in the framework of ECHBM.[14d] Because the N atom has a higher proton affinity than the O atom, the [−N−H···O−] valence bond (VB) form is more stable than the [−N···H−O−] VB and more frequently observable[14c,24] On the basis of these findings the hydrazone tauotmer is expected to be more stable than the azo form, as shown for compounds **3** and **4**. On the other hand, the hydrazone form is destabilized by the loss of the resonance energy on the naphthalene ring (∼25 kcal/mol).[25] Consequently, the two tautomeric forms become energetically close to each other due to the counterbalance between the stability gained through hydrazone type of hydrogen bonding and the resonance energy penalty. Indeed, for **3** and **4**, the electronic energy difference between two tautomers in the gas phase is only 1.1 and 1.0 kcal/mol, respectively. In a similar fashion, hydrazone forms should also be stabilized in compounds **1** and **2** due to the higher proton affinity of nitrogen. However, at this stage the greater resonance energy of benzene ring (∼36 kcal/mol)[25] alters the direction of the equilibrium toward the azo form.

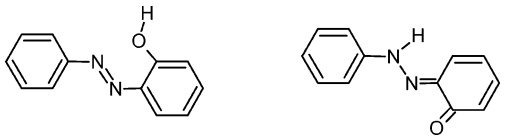

Figure 2. Open forms for the azo and hydrazone tautomers.

The geometric, topological, and energetic parameters of hydrogen bonding in azo and hydrazone tautomers for compounds **1**−**4** are displayed in Table 2.

According to the interpretation of the topological parameters, the negative $\nabla^2\rho(r)$ and high values of $\rho(r)$ at the observed bond critical points correspond to shared or covalent interactions for H···O bond of the compounds **1a**, **2a**, **3a**, and **4a** and for the H···N bond of compounds **1h**, **2h**, **3h**, and **4h**. In each case, properties of electron density at the bond critical points for noncovalent interactions (i.e., H···N bond of the compounds **1a**, **2a**, **3a** and **4a** and H···O bond of the compounds **1h**, **2h**, **3h**, and **4h**) comply with the hydrogen bonding criteria proposed by Popelier[16b] with $\rho(r)$ values within the range 0.002−0.04 au and $\nabla^2\rho(r)$ values within the range 0.02−0.15 au. Existence of a ring critical point in each case has been considered as supporting evidence for the formation of intramolecular hydrogen bonds in these tautomers.

On the other hand, corresponding bond critical points in the transition states **1TS**, **2TS**, **3TS**, and **4TS**, where the proton is placed between the electronegative atoms, have been defined by negative $\nabla^2\rho(r)$ values and relatively higher $\rho(r)$ values than weak intramolecular hydrogen bonds present in the tautomers. Therefore they can be described as shared interactions or covalent bonds and this is generally considered as an evidence for the covalent nature of the resonance-assisted strong hydrogen bonds formed in proton-transfer transition states of compounds **1**−**4**.

The hydrogen bond energies (E_{HB}) have been estimated in two ways: (i) from the difference between the total energy of the hydrogen-bonded molecule and that of its open form, i.e., the form when the donor and acceptor atoms do not see each other (the latter is obtained either by rotating the phenolic hydrogen by 180° for the azo tautomer case or by rotating the C−N bond for the hydrazone tautomer as shown in Figure 2); (ii) from the kinetic energy density, $G(r)$, and $\nabla^2\rho(r)$ obtained by AIM analysis.[24,26] The second methodology is proposed by Espinosa et al.[26a] They found an exponential relationship between the H···O distance and topological parameters such as potential and kinetic energy densities as well as between the H···O distance and dissociation energy for 83 A−H···O (A = C, N, O) hydrogen bonds that were observed experimentally by accurate X-ray diffraction measurements. From these relations they proposed a relationship between the hydrogen bond energy, E_{HB}, and the potential energy electron density, $V(r)$, at H···O bond critical point as $E_{HB} = 0.5V(r)$ because it fits well into the experimental systems considered. $V(r)$ can be calculated by using $\nabla^2\rho(r)$ and $G(r)$ through the virial theorem. Even though this method does not always hold for systems with larger H···O distances like C−H···O[27] interactions (probably because these types of interactions constitute a smaller part of the database hydrogen bond systems used for the fitting), it is a very useful empirical relation for the types of compounds studied here such as N−H···O and O−H···O interactions, especially with H···O distances being less than 2.2 Å.

Hydrogen bond energies estimated by these two methods are not always the same. In the case of the hydrazone tautomers with naphthalene unit (**3h** and **4h**), steric effects and deviation

TABLE 2: Geometric (Bond Distances, Å; Bond Angles, Deg), Topological (au), and Energetic Parameters (kcal/mol) for Hydrogen Bonding in Azo and Hydrazone Tautomers and Proton-Transfer Transition States of Compounds 1−4

	geometric parameters			topological parameters H···N		topological parameters H···O		energetic parameters	
	N···O	H···O a/o H···N	∠ NHO	$\rho(r)$	$\nabla^2\rho(r)$	$\rho(r)$	$\nabla^2\rho(r)$	E_{HB} (via open form)	E_{HB} (via AIM)
1a	2.584	1.707	144.4	0.05329	0.03085	0.32664	−0.46174	12.75	13.11
1TS	2.396	1.270 1.205	150.8	*0.19988*	*−0.17298*	*0.15050*	*−0.03984*		
1h	2.538	1.643	140.0	0.31053	−0.41247	0.05655	0.04062	15.42	15.11
2a	2.574	1.685	145.4	0.05676	0.03092	0.32049	−0.44531	15.80	14.13
2TS	2.404	1.270 1.211	151.4	*0.19153*	*−0.16963*	*0.15083*	*−0.04091*		
2h	2.546	1.642	140.8	0.30921	−0.41071	0.05688	0.04022	16.40	15.15
3a	2.534	1.638	145.4	0.06308	0.03235	0.31521	−0.43092	14.40*	16.61
3TS	2.385	1.211 1.254	150.9	*0.17510*	*−0.11362*	*0.17648*	*−0.09705*		
3h	2.553	1.693	137.2	0.32004	−0.42982	0.05025	0.03821	16.39*	13.19
4a	2.536	1.633	146.0	0.06441	0.03170	0.31166	−0.42095	16.87*	16.96
4TS	2.394	1.217 1.254	151.3	*0.17596*	*−0.11650*	*0.17387*	*−0.09160*		
4h	2.563	1.694	137.9	0.31904	−0.42888	0.05023	0.03769	17.99	13.12

from planarity cause an extra destabilization of the non-hydrogen-bonded open form. Consequently, hydrogen bond energies calculated by using the open forms (16.5 and 18.0 kcal/mol) are much higher than the hydrogen bond energies estimated by the AIM analysis (13.2 and 13.1 kcal/mol). On the other hand, in the case of the hydrazone tautomers with the benzene moiety (**1h** and **2h**), steric effects are not effective and planarity is conserved in the open forms. Therefore, hydrogen bond energies estimated by this method (15.4 and 16.4 kcal/mol) and by the AIM analysis (15.1 and 15.2 kcal/mol) are close to each other.

To understand the difference in hydrogen bond energies obtained by the two methods in **3a**, further AIM analyses were performed on the non-hydrogen-bonded open forms of **1a**−**4a**. In all four cases, (3, −1) bond critical points have been observed between the N and O atoms, corresponding to a heteroatom neighbor interaction,

with a potential energy of 6.6−7.1 kcal/mol. Similar interactions are familiar from another study on noncovalent interactions of the acceptor−donor type of conducting polymers.[28] Also, (3, +1) ring critical points have been observed for this weak interaction. Ring formation provides planarity and stabilizes the open form. However, these bond and ring critical points are present in all azo tautomers and this observation alone is not enough to explain the special case of **3a**. On the other hand, another bond critical point has been located between N and H atom of the naphthalene ring,

but this time only for the case **3a**.This weak interaction (3.1 kcal/mol), also accompanied by a ring critical point, might be the reason for the enhanced planarity and extra stabilization of the open form of **3a**. Therefore, the hydrogen bond energy calculated by this method (14.4 kcal/mol) is lower than the hydrogen bond energy estimated by the AIM analysis (16.6 kcal/mol).

Taking into account these "nonsystematic" extra stabilizations and destabilizations of the open forms, AIM analysis has been found to be a more reliable tool for predicting and comparing the intramolecular hydrogen bond energies of the azo and hydrazone tautomers of **1**−**4**. Gilli et al.[29] have calculated the hydrogen bond energies of the tautomers of compound **3** by employing the open forms of the hydrogen-bonded structures and these values are 15.7 and 14.6 kcal/mol for the hydrazone and azo tautomers, respectively. However, in ref 29 the heteroatom distances and reaction energies (which are very close to the data presented in the present study) are not consistent with the corresponding hydrogen-bond energies. It is possible that the usage of the open forms suffering from steric effects has caused the discrepancy between the hydrogen bond energies and the reaction energies in the study of Gilli et al.[29]

In the present study, the geometric and energetic parameters are consistent with each other as shown in Tables 1 and 2. Transition states possess the strongest hydrogen bonds, hence the highest energy on the potential energy surface and shortest heteroatom−heteroatom (N···O separation less than or equal to 2.404 Å) and proton-heteroatom distances (H···N and H···O distances in the range of 1.205−1.270 Å). Also, note that N···H···O angle in any TS of compounds **1**−**4** is greater than 150°. The corresponding azo and hydrazone tautomers, on the other hand, show relatively weaker hydrogen bonding interactions. N···O distances are comparatively longer and in the range 2.534−2.584 Å. H···N and H···O distance values are also larger and in the range of 1.633−1.707 Å. Moreover, as a tautomer approaches the corresponding transition state over the PES, its hydrogen bond energy increases. This observation is in accord with Hammond's postulate considering that the intramolecular proton-transfer transition state has the strongest hydrogen bond for a given reactant and product and any molecule located energetically close to it will resemble its properties. As stated in transition−state hydrogen bond theory by Gilli et al.[29] the energetically less stable tautomer will have the stronger intramolecular hydrogen bond.

Tables 1 and 2 are also useful in discussing the substituent effect of SO_3^- and the presence of the naphthalene group.[14] Electron-withdrawing substituents in the close proximity decrease the proton affinity of nitrogen and therefore increase and decrease the hydrogen bond strength of the hydrazone and azo tautomers, respectively[14] Because the phenyl ring with a sulfonate group at the para position does not have a very strong electron-withdrawing character, it does not affect the hydrogen

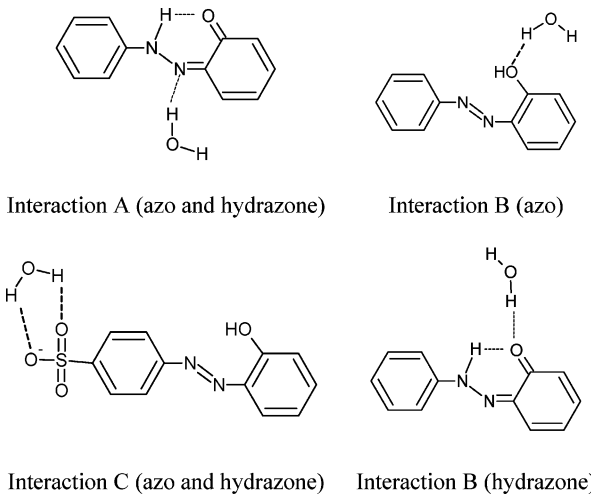

Figure 3. Specific dye−solvent interactions in the first solvation shell.

bonding patterns, hence the stabilities, of the tautomers. The presence of the naphthalene group, however, introduces a more drastic change. Replacing the benzene ring with naphthalene in going from **1** to **3** and from **2** to **4** increases the strength of N···HO by 3 kcal/mol in azo compounds, whereas the NH···O interaction weakens by 2 kcal/mol in hydrazone compounds. Therefore, compounds **3** and **4** exist in their hydrazone tautomers. One important consequence of the trend in stability is the use of advanced oxidation methods for the degradation of the compound **3**. Because compound **3** is abundant mostly in the hydrazone form, hydroxyl radicals will attack the C atom of the H−N−N═C and break the N−C bond. It is very likely that benzene will be the byproduct along the degradation process. Therefore, the advanced oxidation processes for compound **3**, the azo dye Solvent Yellow 14, should be carried out with care.

Environmental Factors Controlling the Azo−Hydrazone Tautomerism. ***The Effect of the Continuum.*** The presence of an electrostatic continuum does not change the general trends in azo−hydrazone tautomerism; i.e., the same trend is observed when switching from gas phase to solution for compounds **1**−**4** (Table 1). However, the hydrazone form is more stabilized in water, for water soluble SO_3^- substituted compounds **2h** and **4h**. In a similar fashion, the azo form is more destabilized in the cases where the solvent destabilization occurs (**1a** and **3a**). Consequently, the energy difference between azo and hydrazone tautomers decreases to 1.6 and 1.5 kcal/mol for phenolic compounds **1** and **2** whereas it increases to 2.6 and 3.0 kcal/mol for naphtholic compounds **3** and **4**. Furthermore, as observed experimentally, the presence of a sulfonate group renders the azo dye water-soluble.[15]

Specific Solute−Solvent Interactions. Continuum solvation models, where the solvent is considered as a uniform polarizable medium with a certain dielectric constant, fail to describe the specific solute−solvent interactions like hydrogen bonding. Therefore, molecular dynamics (MD) simulations have been performed for molecules **1**−**4** to elucidate the specific interactions of solute and solvent molecules.[30] Figure 1S shows the pair correlation functions corresponding to the main intermolecular interactions between the dye and water molecules. Figure 3 summarizes these interactions and shows approximate locations of the explicit water molecules in the first solvation shell obtained by the trajectory analyses.

The individual contribution of each interaction A, B, and C has been investigated by adapting a supermolecule approach. Water-soluble compounds **2** and **4** have been studied for a better understanding of the effect of the naphthalene substitution on stability trends. Hence, supermolecules are composed of dye molecules **2** and **4** and explicit water representing the interactions A, B, or C. Table 3 shows the geometric, topological, and energetic parameters for this partitioning.

The intramolecular hydrogen bond N···H in **2a** has a strength of 14.1 kcal/mol (Table 2). The corresponding values for **2a(A)** and **2a(C)**, as presented in Table 3, are very close to this value: 13.9 and 14.1 kcal/mol, respectively. However, the intramolecular N···H bond in **2a(B)** is much stronger with a value of 16.7 kcal/mol. This is due to the cooperative effect[31] of the intramolecular and intermolecular hydrogen bonds. Because interaction B involves the tautomeric oxygen, it weakens the tautomeric proton−oxygen bond and strengthens the proton−nitrogen interaction, N···H. As a result of this cooperative hydrogen bonding, the azo tautomer **2a(B)** becomes energetically closer to the transition state and the stability difference between the azo and hydrazone tautomers diminishes. In the same manner, in **2h(B)**, the intramolecular H···O bond weakens because the oxygen atom is now interested in sharing its electrons with the hydrogen of the water. However, the negative cooperativity effect[31] in **2h(B)**, where the tautomeric oxygen atom is a double acceptor, is much less pronounced than the cooperativity effect in **2a(B)**, where oxygen is sequentially donor and acceptor for intramolecular and intermolecular hydrogen bonding interactions, respectively and where there is larger amount of polarization. Overall, azo and hydrazone tautomers become isoenergetic on the potential energy surface as a result of the stabilization-destabilization counterbalance introduced by Interaction B. The geometric and topological parameters are consistent with this conclusion. The N···O distance is 2.574 Å in **2a**. The corresponding values in **2a(A)** and **2a(C)** do not change (2.575 and 2.574 Å, respectively). However, the N···O distance is 2.546 Å in **2a(B)**, pointing to a stronger interaction. The H···O distance is also smaller in **2a(B)**, with a value of 1.641 Å. Interaction B also stands for the strongest intermolecular interaction of the present study with hydrogen bonding energy in the range 6.0−7.8 kcal/mol. Also, it is stronger for the hydrazone tautomers than for the azo tautomers by 1.6−1.8 kcal/mol.

This cooperativity effect is also observed in the case of **4a**. The intramolecular hydrogen bond strength for **4a(B)** amounts to 20.3 kcal/mol, and it is 17.0 kcal/mol for **4a**. But in this case the azo tautomer is already located higher in energy than the hydrazone tautomer, and this further decrease in stability results in the further separation of the **4a(B)** and **4h(B)** on the potential energy surface by 3.3 kcal/mol whereas **4a** and **4h** are separated only by 1.0 kcal/mol. Geometric and topological parameters, again, support these findings. The N···O distance of 2.536 Å in **4a** is reduced to 2.506 Å in **4a(B)**. The H···N distance is reduced from 1.633 to 1.585 Å by the inclusion of an explicit water molecule.

In the case of interaction A, the hydrogen bond formation between the unprotonated nitrogen and hydrogen of the solvent water molecules seems to have a semicooperative effect on the intramolecular hydrogen bonding. The intermolecular H−N-**N**···**H**−**O**H hydrogen bond in **2h(A)** might be increasing the strength of the intramolecular **O**···**H**−N−N hydrogen bond because under these conditions the unprotonated nitrogen will probably behave like an electron-withdrawing group next to the tautomeric nitrogen, hence reducing its interest on the proton. This case very much resembles the findings of the study of Gilli et al. where they concluded that the presence of electron-withdrawing or -donating substituents in certain positions affect

TABLE 3: Geometric (Bond Distances, Å; Bond Angles, Deg), Topological (au), and Energetic Parameters (kcal/mol) for Hydrogen Bonding in Azo and Hydrazone Tautomers of Compounds 1−4 with One Explicit Water

	geometric parameters					topological parameters				energetic parameters E_{HB} (AIM)				
	intramolecular			intermolecular		intramolecular H···N/O		intermolecular HOH··N/O		intramolecular		intermolecular		
	N···O	H···O a/o H···N	∠ NHO	N···O	HOH···O a/o HOH···N	$\rho(r)$	$\nabla^2\rho(r)$	$\rho(r)$	$\nabla^2\rho(r)$	H···N	H···O	H···N	H···O	relative energy[a]
2aA	2.575	1.690	145.1	2.998	2.033	0.05591	0.03109	0.02477	0.01509	13.92		4.96		7.67 (2.96)
2aB	2.546	1.641	146.3	2.891	1.922	0.06328	0.03098	0.02539	0.01886	16.40			5.98	7.62 (2.21)
2aC	2.574	1.686	145.3	2.934	2.099	0.05652	0.03095	0.01999	0.01426	14.06			4.91	**0 (0)**
				2.930	2.090			0.01966	0.01407					
2hA	2.528	1.612	142.0	3.027	2.065	0.06112	0.04212	0.02273	0.01434		16.71	4.59		11.28 (5.14)
2hB	2.552	1.659	140.0	2.800	1.819	0.05432	0.03946	0.03379	0.02404		14.37		7.76	7.76 (1.64)
2hC	2.542	1.637	141.0	2.936	2.101	0.05756	0.04041	0.01911	0.01374		15.40		4.68	2.61 (1.56)
				2.943	2.115			0.01963	0.01402					
4aA	2.532	1.633	145.8	3.164	2.192	0.06437	0.03214	0.01692	0.01950	17.04		3.41		10.14 (7.48)
4aB	2.506	1.585	147.0	2.888	1.920	0.07284	0.03015	0.01901	0.01888	20.29			6.01	8.81 (4.97)
4aC	2.534	1.632	146.0	2.933	2.095	0.06460	0.03178	0.01977	0.01414	17.06			4.85	1.11 (2.72)
				2.933	2.096			0.01975	0.01412					
4hA	2.549	1.675	138.3	3.209	2.239	0.05241	0.03923	0.01504	0.01011		13.86	3.17		9.71 (5.31)
4hB	2.564	1.703	137.2	2.806	1.827	0.04898	0.03734	0.03312	0.02356		12.83		7.61	5.55 (0.46)
4hC	2.561	1.693	137.9	2.930	2.092	0.05034	0.03786	0.01992	0.01421		13.18		4.89	**0 (0)**
				2.931	2.093			0.01988	0.01419					

[a] 0.00 kcal/mol in the relative energy data corresponds to the lowest energy tautomer for compounds **2** and **4** as follows [in Hartrees and in the format of (B3LYP/6-31+G(d,p), IEFPCM//B3LYP)]: **2aC** = (−1347.79434105, −1347.860736), **4hC** = (−1501.4473592, −1501.513862).

TABLE 4: Geometric (Bond Distances, Å; Bond Angles, Deg), Topological (au), and Energetic Parameters (kcal/mol) for Hydrogen Bonding in Azo and Hydrazone Tautomers and Proton-Transfer Transition States of Compounds 2 and 4 with Three Explicit Water Molecules

				2a(ABC)	**2TS(ABC)**	**2h(ABC)**	**4a(ABC)**	**4TS(ABC)**	**4h(ABC)**
geometric parameters	intramolecular		N···O	2.548	2.396	2.537	2.505	2.387	2.553
			H···N a/o H···O	1.650	1.229	1.636	1.589	1.278	1.691
					1.243			1.187	
			∠NHO	145.8	151.5	140.7	146.7	151.2	137.3
	intermolecular	interaction A	N···O	3.006	3.019	3.045	3.163	3.161	3.234
			HOH···N	2.054	2.068	2.098	2.193	2.191	2.264
		interaction B	O···O	2.898	2.843	2.811	2.898	2.858	2.817
			HOH···O	1.930	1.868	1.831	1.935	1.889	1.841
		interaction C	O···O	2.928	2.927	2.925	2.9312.937	2.929	2.930
				2.945	2.944	2.944		2.938	2.935
			HOH···O	2.084	2.084	2.083	2.095	2.091	2.093
				2.120	2.120	2.121	2.104	2.109	2.104
topological parameters	intramolecular		$\rho(r)$ H···N a/o H···O	0.06164	0.18846	0.05734	0.07192	0.16469	0.05039
					0.16131			0.18738	
			$\nabla^2\rho(r)$	0.03141	−0.14698	0.04119	0.03090	−0.09094	0.03848
					−0.06301			−0.12129	
	intermolecular	interaction A	$\rho(r)$	0.02363	0.02268	0.02114	0.01677	0.01677	0.01419
			$\nabla^2\rho(r)$	0.01460	0.01432	0.01357	0.01096	0.01102	0.00967
		interaction B	$\rho(r)$	0.02493	0.02952	0.03275	0.02474	0.02803	0.03208
			$\nabla^2\rho(r)$	0.01853	0.02135	0.02331	0.01833	0.02034	0.02281
		interaction C	$\rho(r)$	0.02022	0.02022	0.02030	0.01946	0.01931	0.01951
				0.01888	0.01888	0.01889	0.01982	0.01990	0.01991
			$\nabla^2\rho(r)$	0.01440	0.01443	0.01446	0.01398	0.01391	0.01401
				0.01366	0.01367	0.01367	0.01420	0.01428	0.01424
energetic parameters	intramolecular		H···N a/o H···O	15.90	*90.78*	15.44	20.03	*74.21*	13.28
			H···O		*79.03*			*98.98*	
	intermolecular	interaction A	H···N	4.76	4.59	4.30	3.39	3.39	2.86
		interaction B	H···O	5.89	6.86	7.54	5.86	6.55	7.39
		interaction C	H···O	4.96	4.97	4.99	4.78	4.74	4.79
				4.63	4.63	4.64	4.87	4.90	4.89
	relative energy[a]			**−3.15**	**0**	**−2.01**	**−1.40**	**0**	**−4.12**
				(−3.06)	**(0)**	**(−2.83)**	**(−1.18)**	**(0)**	**(−5.04)**

[a] Values in parentheses correspond to the IEFPCM calculations representing the bulk solvent effect.

the strength of the strong hydrogen bonds.[14e] Only this time we do not have covalently bonded substituents but instead groups with strong noncovalent interactions. Interaction A, however, is less effective than interaction B in terms of the cooperative hydrogen bonding for compound **2** because there is no sequentiality of acceptor and donor atoms and it becomes insignificant for compound **4** probably due to the steric effects. The water molecules cannot approach the unprotonated nitrogen atom well enough because of the presence of the bulky naphthalene group. Consequently, intermolecular hydrogen bond

involving interaction A is weaker for tautomers of compound **4** (3.2−3.4 kcal/mol) rather than for those of compound **2** (4.6−5.0 kcal/mol). Comparison of the intermolecular geometric parameters for **2h(A)** and **4h(A)** also supports this idea (Table 3).

Interaction C is not a part of the intramolecular−intermolecular cooperative hydrogen bonding as in the case of interactions A and B. However, two hydrogens of one water molecule interact with two oxygens of the SO_3 group, resulting in a double hydrogen bond,

AIM analysis of these special interactions has shown ring and cage critical points. Therefore, interaction C gives the lowest energy structures and contributes to the stabilization of each tautomer equally. The energy difference between **2a** and **2h** (2.7 kcal/mol) is the same as the one between **2a(C)** and **2h(C)** (2.6 kcal/mol). Similarly, the energy difference between **4a** and **4h** (1.0 kcal/mol) is the same as the energy diference between **4a(C)** and **4h(C**) (1.1 kcal/mol). Also, note that the geometric and topological parameters of the intramolecular hydrogen bonding are conserved even after inclusion of Interaction C.

An interesting feature of the MD simulations with the azo tautomers of **1a**-**4a** is the occasional free rotation of the phenolic proton around the C−O bond, a behavior that is tracked by monitoring the C−C−O−H dihedral angle throughout the trajectory. This effect is more prominent in the case of SO_3 substituted azo tautomers, **2a** and **4a** as a sign of weakened intramolecular hydrogen bond N···HO with respect to the unsubstituted azo tautomer. In these latter cases, the rotating proton is capable of making intermolecular hydrogen bonds with the surrounding water molecules, as confirmed by the pair correlation function between the proton and oxygen atoms of the water. DFT calculations have predicted a hydrogen bond energy of 6.7 kcal/mol corresponding to this intermolecular interaction for compound **4a**. Heteroatom−heteroatom interaction between the tautomeric nitrogen and oxygen, in the absence of proton in between, has a potential energy contribution of 6.5 kcal/mol to the bond critical point. A ring critical point observed by AIM analysis of the electron density may be responsible for the conservation of the planarity of the dye during this rotation.

The geometric, topological, and energetic parameters of intramolecular and intermolecular hydrogen bonding for azo and hydrazone tautomers and proton-transfer transition states with three explicit water molecules (representing the combined interactions of A, B, and C) are gathered in Table 4. Figure 4 shows the optimized structures for compound **4(ABC)**.

The effect of specific solute−solvent interactions in the first solvation shell on the azo−hydrazone tautomerism can be examined by the comparison of Tables 1 and 4. The energy difference between **2a** and **2h** is 2.7 kcal/mol (Table 1), whereas this difference is only 1.1 kcal/mol between **2a(ABC)** and **2h(ABC)** (Table 4). In continuum, the corresponding energy differences are 1.5 kcal/mol for the former pair and 0.2 kcal/mol for the latter. The tautomers of Acid Orange 7 **4a** and **4h** are close in energy (1.0 kcal/mol); however, the corresponding structures with explicit water molecules, **4a(ABC)** and **4h(ABC)**, are separated by 2.7 kcal/mol. This value increases to 3.9 kcal/mol in continuum and is close to the value of the stripped molecules in continuum (3.0 kcal/mol). Examination of the geometric parameters shows that B is the dominant

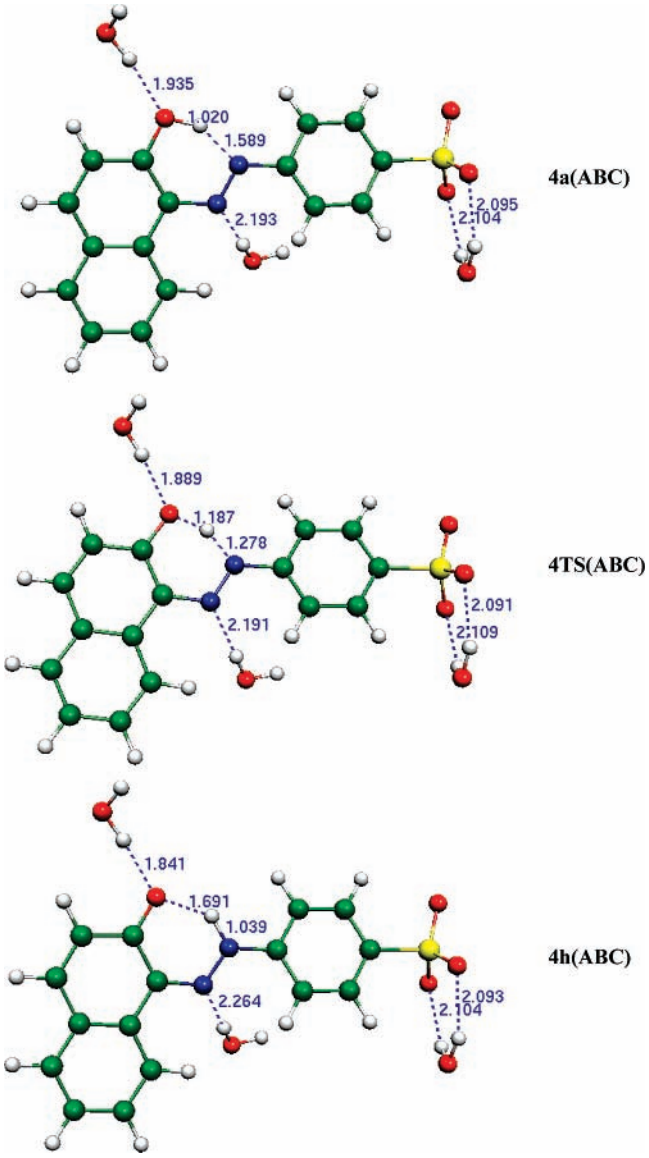

Figure 4. Optimized structures for the azo−hydrazone tautomerism of **4a(ABC)** and **4h(ABC)**.

intermolecular interaction in compounds **2a(ABC)** and **4a(ABC)**. Intramolecular hydrogen bond energy increases by 1.8 and 3 kcal/mol, respectively, for these two tautomers by the inclusion of the explicit water molecules whereas it does not change much for tautomers **2h(ABC)** and **4h(ABC)**.

When the geometries of the transition states are compared, it has been observed that the transition state for compound **2** becomes more symmetrical by the inclusion of explicit water molecules. The N···O distance is reduced to 2.396 Å from its initial value of 2.404 Å. The H···O and H···N distances become 1.243 and 1.229 Å, respectively, as compared to their initial values of 1.270 and 1.211 Å. On the other hand, the transition state for compound **4** loses its symmetrical structure by the inclusion of explicit water molecules. The N···O distance is reduced to 2.387 Å starting from its initial value of 2.394 Å. The H···O and H···N distances become 1.187 and 1.278 Å, respectively, as compared to the initial values of 1.217 and 1.254 Å. A more symmetrical transition state is in agreement with the isoenergetic nature of the tautomers for compound **2**. Similarly, distortion from symmetry for the transition state of **4** explains the stability difference between the azo and hydrazone tautomers for this compound.

It can be concluded that specific solute−solvent interactions affect the intramolecular hydrogen bonding and, hence, the stability of the tautomers. While specific solute−solvent interactions render the tautomers of compound **2** isoenergetic, they increase the energy difference between the tautomers for compound **4** by contributing to the destabilization of the azo tautomer. This computational result is in agreement with the UV−visible spectrum[13c,32] of compound **4**, which shows a peak around 500 nm corresponding to the hydrazone tautomer with a small shoulder around 420 nm corresponding to the azo tautomer.

Both the gas-phase and solvent calculations in this study are in accord with the previous experimental studies for compounds **1**, **3**, and **4**.[33−35] Sullivan et al.[33] have studied the effect and extent of azo−hydrazone tautomerism in azo dyes using electrospray tandem mass spectrometry and MALDI post-source decay mass spectrometry. They found the hydrazone tautomer to be the more stable form for compound **4**. For compounds **3** and **4**, Hihara et al.[36] also found the hydrazone tautomers to be more stable in water using semiempirical PM5 and COSMO methods. However, in the gas phase, they found a lower heat of formation for the azo tautomers, leading to different stability trends in the gas phase and in solution, which is contrary to the arguments presented here and also in the study of Gilli et al. for compound **3**.[14e]

Conclusion

Azo−hydrazone tautomerism in azo dyes has been modeled by using density functional theory (DFT) and atoms-in-molecules analysis of electron density. In the gas phase, the most stable tautomer is the azo compound for model compounds with a phenyl group; however, the hydrazone form is more stable for azo dyes Acid Orange 7 and Solvent Yellow 14 when the naphthyl group replaces the phenyl. Sulfonate group substitution increases the solubility of the compound in water, whereas it does not affect the stability trends of the tautomers. Evolution of the intramolecular hydrogen bond with changing structural and environmental factors during the proton-transfer reaction has provided valuable information on the azo−hydrazone tautomerism. Resonance assisted strong hydrogen bonding properties within the framework of *electrostatic-covalent hydrogen bond model* (ECHBM) were observed at the transition structure formed during the proton-transfer reaction. Overall, similar stability trends have been observed both in the gas phase and in water for all compounds. Special solute−solvent interactions have been further investigated by means of quantum mechanical calculations after defining the first solvation shell by molecular dynamics simulations. Specific solute−solvent interactions have been found to enhance the effect of the electrostatic continuum. Among them, the cooperative hydrogen bonding of the tautomeric oxygen with solvent molecules affects the intramolecular hydrogen bonding most, hence enhancing or decreasing the stability of a certain tautomer but never altering the direction of stability.

Acknowledgment. We thank Boğaziçi Üniversitesi Bilimsel Araştırma Projeleri (BAP 02B501, 03R104) and Devlet Planlama Teşkilatı (DPT 98K 120900) for financial support. P.D. and V.A. acknowledge partial support by COSBIOM Project (EU-FP6-ACC-2004-SSA-2 contract no. 517991) and DPT Project 03K120250.

Supporting Information Available: Table of thermodynamic properties. Figure for pair correlation functions corresponding to the main intermolecular interactions between the dye and water molecules. This information is available free of charge via the Internet at http://pubs.acs.org.

References and Notes

(1) Vinodgopal, K.; Kamat, P. V. In *Environmental Applications of Ionizing Radiation*; Cooper, W. J., Curry, R. D., O'Shea, K. E., Eds.; John Wiley & Sons: New York, 1998; pp 587−599.

(2) Ince, N. H.; Tezcanli, G.; Belen, R. K.; Apikyan, I. G. *Appl. Catal. B: Environ.* **2001**, *29*, 167−176.

(3) Padmaja, S.; Madison, S. A. *J. Phys. Org. Chem.* **1999**, *12*, 221−226.

(4) Kuo, W. G. *Water Res.* **1992**, *26*, 881−886.

(5) Turchi, C. S.; Ollis, D. F. *J. Catal.* **1990**, *122*, 178−192.

(6) Zollinger, H. *Colour Chemistry. Synthesis, Properties and Application of Organic Dyes and Pigments*; VCH: Weinheim, 1991; pp 45−68.

(7) Joseph, J. M.; Destaillats, H.; Hung, H.; Hoffmann, M. R. *J. Phys. Chem. A* **2000**, *104*, 301−307.

(8) Spadaro, J. T.; Isabelle, L.; Renganathan, V. *Environ. Sci. Technol.* **1994**, *28*, 1389−1393.

(9) Kelemen, J. *Dyes Pigm.* **1981**, *2*, 73−91.

(10) Kelemen, J.; Moss, S.; Sauter, H.; Winkler, T. *Dyes Pigm.* **1982**, *3*, 27−47.

(11) Ball, P.; Nicholls, C. H. *Dyes Pigm.* **1982**, *3*, 5−26.

(12) Liebermann, C. *Chem. Ber.* **1883**, *16*, 2858−2864.

(13) (a) Ozen, A. S.; Aviyente, V.; Klein, R. A. *J. Phys. Chem. A* **2003**, *107*, 4898−4907. (b) Ozen, A. S.; Aviyente, V.; De Proft, F.; Geerlings, P. *J. Phys. Chem. A* **2004**, *108*, 5990 -6000. (c) Ozen, A. S.; Aviyente, V.; Tezcanli-Guyer, G.; Ince, N. H. *J. Phys. Chem. A* **2005**, *109*, 3506−3516.

(14) (a) Gilli, G.; Bellucci, F.; Ferretti, V.; Bertolasi, V. *J. Am. Chem. Soc.* **1989**, *111*, 1023−1028. (b) Gilli, P.; Bertolasi, V.; Ferretti, V.; Gilli, G. *J. Am. Chem. Soc.* **1994**, 116, 909−915. (c) Gilli, P.; Bertolasi, V.; Ferretti, V.; Gilli, G. *J. Am. Chem. Soc.* **2000**, *122*, 10405. 10417. (d) Gilli, G.; Gilli, P. *J. Mol. Struct.* **2000**, *552*, 1−15. (e) Gilli, P.; Bertolasi, V.; Pretto, L.; Lycka, A.; Gilli, G. *J. Am. Chem. Soc.* **2002**, *124*, 13554−13567. (f) Gilli, P.; Bertolasi, V.; Pretto, L.; Ferretti, V.; Gilli, G. *J. Am. Chem. Soc.* **2004**, *126*, 3845−3855.

(15) (a) Bader, R. F. W. *Atoms in Molecules: A Quantum Theory*; International Series of Monographs on Chemistry; Clarendon Press: Oxford, U.K., 1995; Vol. 22, pp 1−438. (b) Bader, R. W. F. *Chem. Rev.* **1991**, *91*,893−928 (c) Popelier, P. *Atoms in Molecules An Introduction*; Pearson Education Limited: London, England, 2000.

(16) (a) Material Safety Data Sheets, ScienceLab.com, Inc., Houston, TX, US, 2005. (b) Material Safety Data Sheets and Technical Information, BASF Corp., Charlotte, NC.

(17) Frisch, M. J.; Trucks, G. W.; Schlegel, H. B.; Scuseria, G. E.; Robb, M. A.; Cheeseman, J. R.; Montgomery, J. A., Jr.; Vreven, T.; Kudin, K. N.; Burant, J. C.; Millam, J. M.; Iyengar, S. S.; Tomasi, J.; Barone, V.; Mennucci, B.; Cossi, M.; Scalmani, G.; Rega, N. G.; Petersson, A.; Nakatsuji, H.; Hada, M.; Ehara, M.; Toyota, K.; Fukuda, R.; Hasegawa, J.; Ishida, M.; Nakajima, T.; Honda, Y.; Kitao, O.; Nakai, H.; Klene, M.;Li, X.; Knox, J. E.; Hratchian, H. P.; Cross, J. B.; Adamo, C.; Jaramillo, J.; Gomperts, R.; Stratmann, R. E.; Yazyev, O.; Austin, A. J.; Cammi, R.; Pomelli, C.; Ochterski, J. W.; Ayala, P. Y.; Morokuma, K.; Voth, G. A.; Salvador, P.; Dannenberg, J. J.; Zakrzewski, V. G.; Dapprich, S.; Daniels, A. D.; Strain, M. C.; Farkas, O.; Malick, D. K.; Rabuck, A. D.; Raghavachari, K.; Foresman, J. B.; Ortiz, J. V.; Cui, Q.; Baboul, A. G.; Clifford, S.; Cioslowski, J.; Stefanov, B. B.; Liu, G.; Liashenko, A.; Piskorz, P.; Komaromi, I.; Martin, R. L.; Fox, D. J.; Keith, T.; Al-Laham, M. A.; Peng, C. Y.; Nanayakkara, A.; Challacombe, M.; Gill, P. M. W.; Johnson, B.; Chen, W.; Wong, M. W.; Gonzalez, C.; Pople, J. A. *Gaussian 03*, revision B.04; Gaussian, Inc.: Pittsburgh, PA, 2003.

(18) Tomasi, J.; Mennucci, B.; Cancés, E. *J. Mol. Struct. (THEOCHEM)* **1999**, *464*, 211−226.

(19) Shi, S.; Yan, L.; Yang, Y.; Fisher-Shaulsky, J.; Thacher, T. *J. Comput. Chem.* **2003**, *24*, 1059−76.

(20) Accelrys Inc, San Diego, CA, U.S.A. (Insight II 4.0.0 P+, Discover3, Amorphous_Cell, and Builder Modules version 2001.11).

(21) (a) Biegler-König, F. *J. Comp. Chem.* **2000**, *21*, 1040−1048. (b) Bielkgler-König, F.; Schönbohm, J.; Bayles, D. *J. Comput. Chem.* **2001**, *22*, 545−559.

(22) Portman, S. MOLEKEL Version 4.3.win32, www.cscs.ch/molekel/.

(23) Kumar, G. A.; Pan, Y.; Smalwood, C. J.; McAllister, M. A. *J. Comput. Chem.* **1998**, *19*, 1345−1352.

(24) Sobczyk, L.; Grabowski, S. J.; Krygowski, T. M. *Chem. Rev.* **2005**, *105*, 3513−3560.

(25) Carey, F.A. *Organic Chemistry*, 4th ed.; McGraw-Hill Higher Education: Boston, 2002.

(26) (a) Espinosa, E.; Molins, E.; Lecomte, C. *Chem. Phys. Lett.* **1998**, *285*, 170−173. (b) Espinosa, E.; Molins, E. *J. Chem. Phys.* **2000**, *113*, 5686.

(27) Gatti, C.; May, E.; Destro, R.; Cargnoni, F. *J. Phys. Chem. A* **2002**, *106*, 2707−2720.
(28) Ozen, A. S.; Sonmez, G.; Atilgan, C. *J. Phys. Chem. C* **2007**, *111*, 16362−16371.
(29) Gilli, P.; Bertolasi, V.; Pretto, L.; Antonov, L.; Gilli, G. *J. Am. Chem. Soc.* **2005**, *127*, 4943−4953.
(30) Tomasi, J.; Mennucci, B.; Cammi, R. *Chem. Rev.* **2005**, *105*, 2999.
(31) Scheiner, S. *Hydrogen bonding A Theoretical Perspective*; Oxford Unversity Press: New York, 1997.
(32) Galindo, C.; Jacques, P.; Kalt, A. *J. Adv. Oxid. Technol.* **1999**, *4*, 400−407.
(33) Sullivan, A. G.; Garner, R.; Gaskell, S. J. *Rapid Commun. Mass Spectrom.* **1998**, *12*, 1207−1215.
(34) Uno, T.; Kim, B.; Machida, K.; Uno, T. *Bull. Chem. Soc. Jpn.* **1974**, *47*, 2111.
(35) Kuder, J. E. *Tetrahedron* **1972**, *28*, 1973.
(36) Hihara, T.; Okada, Y.; Morita, Z. *Dyes Pigm.* **2003**, *59*, 25−41.